FAST BIAS FIELD CORRECTION FOR 9.4 TESLA MAGNETIC RESONANCE IMAGING

X. Peña Piña[1], M. Bach Cuadra[1], N. Kunz[2], N. Just[2], R. Gruetter[2] and J.-Ph. Thiran[1]

[1]Signal Processing Laboratories (LTS5)
[2]Laboratory of Functional and Metabolic Imaging (LIFMET)

Ecole Polytechnique Fédérale de Lausanne (EPFL), CH-1015 Lausanne, Switzerland
Email: {xavier.penya,meritxell.bach,nicolas.kunz,nathalie.just,rolf.gruetter,jp.thiran}@epfl.ch

ABSTRACT

In this paper the problem of intensity inhomogeneity at high magnetic field on magnetic resonance images is addressed. Specifically, rat brain images at 9.4T acquired with a surface coil are bias corrected. We propose a low-pass frequency model that takes into account not only background-object contours but also other important contours inside the image. Two pre-processing filters are proposed: first, to create a volume of interest without contours, and second, to extrapolate the image values of such masked area to the whole image. Results are assessed quantitatively and visually in comparison to standard low pass filter approach, and they show as expected better accuracy in enhancing image intensity.

1. INTRODUCTION

Magnetic Resonance Imaging (MRI) is mainly used in the clinical practice as a powerful non-invasive diagnostic tool. It has also a fundamental importance in preclinical research [1], which recently has further evolved towards different magnetic fields: 9.4 and 14.1 Tesla (T) for animals, while human magnets can be of range 1.5T, 3T and 7T. Higher field strength improves either the Signal to Noise Ratio (SNR) or acquisition time. But at high magnetic field, the intensity inhomogeneity (IIH) effect, also called bias field, is also more important [2]. To correct for such artifact is necessary for further image analysis using computer vision techniques or even visual inspection. In this work the problem of bias correction at high magnetic field is addressed. Specifically, rat brain images at 9.4T acquired with a surface coil (where the inhomogeneity is stronger than in volume coils) will be used.

Most of the research work [3, 4] done so far about bias field correction is related to $1.5T$ and $3T$ devices. The existing methods can be classified into four main groups:

- *Low-frequency model.* The bias, under smoothness assumption, is confined in the low frequency range of the acquired image. Thus, low-pass filtering [5, 6] is used to estimate the bias.
- *Hypersurface model.* These methods estimate analytically the bias by a smooth functional model [7]. Their degree of complexity is higher than a low-frequency model.
- *Statistical model.* This type of model assumes the bias to be a random variable, and it uses statistical estimation to remove the bias from the data set[8, 9].
- *Information acquired with other MR scans.* It consists in acquiring extra information during the imaging process such as a RF map[10], or capturing an image with a body coil to help correct the surface coil image [11].

In this paper we have chosen the low-frequency model to estimate the bias by means of low-pass filtering, due to its main two advantages: its speed and its low computation complexity. However their efficiency is typically limited because of the *edge effects* related to high image contrasts [4]. In this work we try to palliate for these effects, not only for object-background transitions [5, 12, 13, 14] but also for other high frequencies present in the image. First, a brief mathematical description of the image model is performed in Section 2. The low-frequency model limitations are presented in Section 3. Our proposed solution is developed in Section 4. Results and qualitative validation are done in Section 5. Section 6 concludes this work.

2. MATHEMATICAL MODEL

Due to the nature of the MR acquisition, the bias field is modeled as a multiplicative function, spread all through the image:

$$s(\underline{x}) = o(\underline{x}) \cdot b(\underline{x}) + n(\underline{x}), \tag{1}$$

where $s(\underline{x})$ is the acquired image, $o(\underline{x})$ is the ideal image with no bias, $b(\underline{x})$ is the bias field ($0 < b(\underline{x}) < 1$) and $n(\underline{x})$ represents all the noise present in the system. This noise is usually considered additive and gaussian. $\underline{x} = (x, y, z)$ represents the position pixel position[1].

The usual procedure to alleviate this intensity inhomogeneity is:

- First, estimate the bias field $b(\underline{x})$ (this estimation will be referred in this paper as $\hat{b}(\underline{x})$).
- Then, divide the biased image $s(\underline{x})$ by the estimated

This work is supported by the Center for Biomedical Imaging (CIBM) of the Geneva - Lausanne Universities and the EPFL, and the foundations Leenaards and Louis-Jeantet.

[1]Another usual approach is to translate the problem into the logarithmic domain, where the bias term becomes additive $log(s(\underline{x})) \approx log(o(\underline{x})) + log(b(\underline{x}))$.

bias $\hat{b}(\underline{x})$, obtaining as a result:

$$\frac{s(\underline{x})}{\hat{b}(\underline{x})} = \frac{o(\underline{x}) \cdot b(\underline{x}) + n(\underline{x})}{\hat{b}(\underline{x})} \approx o(\underline{x}) + \frac{n(\underline{x})}{b(\underline{x})}. \quad (2)$$

Thus, we can observe how the correction enhances the noise. As the range of values of the bias field is $0 < b(\underline{x}) < 1$, the resulting noise becomes:

$$n'(\underline{x}) = \frac{n(\underline{x})}{b(\underline{x})} > n(\underline{x}). \quad (3)$$

3. LIMITATIONS OF THE LOW-FREQUENCY MODEL

3.1 Background noise

As assumed in Eq. 1, there is no bias contribution to the noise, $n(\underline{x})$, and thus it is not useful for bias estimation. Then, bias correction tries to avoid background area. The most common solution is to directly threshold the biased image, setting the threshold at a certain percentage (10% [7] or 15% [12]) of the image intensity histogram. However, as the bias field has a strong influence on the histogram of the image, a more flexible method is needed. Furthermore, in high bias conditions, the task of separating both background noise and highly biased zones becomes much more difficult, since both of them may have similar intensity characteristics. This can be seen in the SNR:

$$SNR(\underline{x}) = \frac{S \cdot b(\underline{x})^2}{N}, \; 0 < b(\underline{x}) < 1, \quad (4)$$

considering a constant noise power N, as well as a constant signal power S. We will take into account all these factors when masking our image.

3.2 Image contours

Image contours (such as brain-skull contours) might distort bias estimation since low-pass filtering mix two different regions, and thus the estimated low frequency variation does not correspond the bias field. Homomorphic un-sharp masking [5] tries to solve this problem by using a band notch filter but its accuracy strongly depends on window size of the filter. Another existing solution [12] is to set background intensity to the mean value of all image voxels but such approach tackles the object-background contour only. Similarly to the extrapolation presented in [13, 14], in this paper we propose to solve this problem from a different point of view, by simply removing and re-filling those transitions relying on their surrounding voxels.

4. METHODOLOGY

Two additional steps are added to a typical low-pass filter estimation and bias removal processing chain (Fig. 7): the *mask filter* and the *expansion filter*. The aim of the mask filter is to remove background and contours as mentioned in Section 3. After that, the expansion filter fills the masked zones. Then, the image is ready for the low pass filter in order to estimate the bias field[2]. We will illustrate our method on a set of *2D* MR acquisitions (surface coil, 9.4T) of a rat brain, assuming that the bias field is constant in z-direction (across slices). Image volume is $512 \times 512 \times 32$ voxels of $0.043 \times 0.043 \times 0.800 mm^3$ resolution. Due to low depth resolution in the z direction, most of the following steps treat each slice independently.

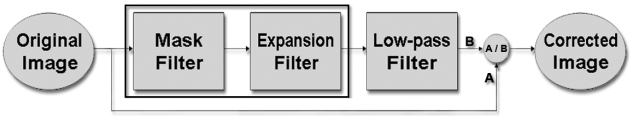

Figure 1: Bloc diagram of the method proposed.

4.1 Mask Filter

4.1.1 Background removal

The first step consists in estimating a SNR map of the image. To this end, the intensity mean, $\hat{\mu}(\underline{x})$, for every pixel, $\underline{x}$, and its $1st$-order neighborhood in 2D (8th neighbors) is computed first. The maximum intensity difference across the values within the window, $MaxDif(\underline{x})$ is also computed. Then, the SNR estimator can be build as:

$$\hat{SNR}(\underline{x}) = (\frac{A_{signal}(\underline{x})}{A_{noise}(\underline{x})})^2 \approx (\frac{\hat{\mu}(\underline{x})}{MaxDif(\underline{x})})^2, \quad (5)$$

where A is the amplitude of the signal. Background is segmented by means of a threshold set by the user on this SNR map. Note that the SNR map can vary significantly depending on the acquisition, and thus the threshold level will vary as well. We select such threshold arbitrarily on the middle slice of the data set and we apply it for the whole volume (we assume noise power to be constant all through the volume). The intensity profile across y-direction in a 2D slice and the selected threshold are shown in Fig. 2(a).

4.1.2 Contour removal

Removal of contours is done by applying a threshold to the intensity image gradient. Mathematically,

$$\begin{aligned} \nabla s(\underline{x}) = \nabla(o(\underline{x}) \cdot b(\underline{x})) + \nabla n(\underline{x}) = \\ \nabla o(\underline{x}) \cdot b(\underline{x}) + o(\underline{x}) \cdot \nabla b(\underline{x}) + \nabla n(\underline{x}) \approx \\ \nabla o(\underline{x}) \cdot b(\underline{x}) + \nabla n(\underline{x}), \end{aligned} \quad (6)$$

since we assume that $\nabla b(\underline{x}) \approx 0$ because of its smooth variation. Thus, note that we apply a threshold on a *biased* intensity gradient $\nabla s(\underline{x})$ and this may cause some non-desired patches to remain attached to the brain (see next subsection). Again, threshold selection varies for different volumes and it is set by the user (seen Fig. 2).

4.1.3 Brain extraction

Our ultimate goal is to be able to obtain a single class object (the rat brain), where bias field will be estimated.

[2]Some methods skip the log transform before applying the low pass filter [5] because they assume that bias field is kept in the lowest frequency band in both domains.

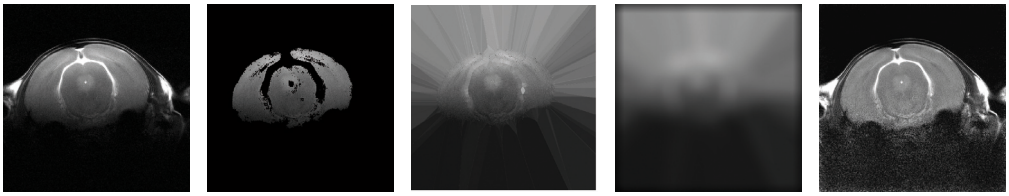

(a) (b) (c) (d) (e)

Figure 3: Original image (a), masked image (b), expanded image (c), low-pass filter (d), and corrected image (e).

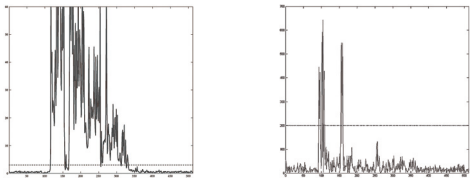

(a) (b)

Figure 2: SNR profile with threshold level marked (a), and gradient profile with its correspondent threshold level (b). The gradient profile has been already masked by the SNR mask.

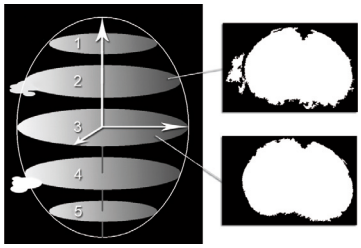

Figure 4: *3D* scheme, slices 2 and 4 contain non-masked artifacts. These artifacts are outside the region delimited by slice 3.

After applying background and contour thresholds, a rough mask has been obtained, thus some non-brain patches could still remain attached to the brain or isolated in the background. For this reason, we will first assume the brain to be the largest compact element in the data set, and this is valid either for the whole *3D* volume and for each separate slice. So image processing is applied in order to keep only the biggest connected object (1st-neighborhood system) for each slice. To ensure that non-brain patches are not attached to the largest volume (particulary in slices with low SNR): we approximate the rat brain by a *3D* ellipse (see Fig. 4). Assuming that the brain extraction in the middle slice is good, then the mask of the following slices must be at least contained inside each other[3]. This concept is visually explained in Fig. 4. The final result of the whole mask filter is shown in Fig. 5.

4.2 Expansion Filter

At this point we have a well-defined brain area, but low-pass filter can not be applied yet, due to background

[3]The rat brain must be vertically aligned along z axis.

Figure 5: Axial, coronal and sagittal views of the mask obtained, it has been kept as discrete along z in order to make clear the gap between slices.

presence and inner holes (see Fig. 3(b)). In order to fulfil these zones the following processing is performed: for every pixel in masked area we assume the bias to be constant and equal to the bias affecting the closest non-masked pixel. So, no assumptions about the bias shape are done but a continuity constraint. The process for every slice is as follows

- A Euclidian distance map $D(\underline{x})$ to the binary mask is computed.
- The gradient, (∇_x, ∇_y), of this distance map is computed.
- Every pixel outside the mask (x, y) will recieve the pixel value located at (x', x'), where

$$\begin{aligned} x' &= x - D(x) \cdot \nabla_x(x) \\ y' &= y - D(x) \cdot \nabla_y(x). \end{aligned} \tag{7}$$

The result of this expansion filter is shown in Fig. 3(c). The artificial contours of this expansion will be compensated by the final low-pass filter. These contour gaps are directly related to the noise inside the brain, and thus the application of this low-pass filter must be homogeneous all over the expanded image.

4.3 Bias estimation and correction

At this point most of the high frequencies present in the original image have been deleted. Therefore, low-pass filter parameters such as window size are now less critical and can be easily selected. Here we will apply as an example a Gaussian filter to estimate the bias from our image (Fig. 3(c)). We set the filter window size to 50×50 pixels and $\sigma = 16$ pixels. No smoothing is used in the z direction. The result of this filter is shown in Fig. 3(d). In order to remove the bias, the corrupted image is divided by the bias estimation, as seen in Fig. 3(e).

5. RESULTS

5.1 Synthetic data

The contribution of our mask and expansion filter (here denoted by *constant* expansion) is analyzed by comparison with the expansion proposed in [13] (here denoted by *mirror* expansion). The low-pass filter used for this comparison is the Wiener filter, due to its advantages in conditions of gaussian noise. We will analyze the results as a function of the window size of this filter (that is the m-by-m neighborhood used to estimate the local image mean and standard deviation).

In order to obtain quantitative results a 2D synthetic phantom is built (Fig. 6(a)), simulating the shape, the bias and the noise of a real acquisition (Fig. 3(a)). We create a ground truth image, Fig. 3(a), with gray values 2200, 1300 and 700. We assume, as described in Eq. 1, a multiplicative bias with a linear variation, as shown in Fig. 8(c). Finally, Gaussian noise is added ($\sigma = 112$). The tests are computed using three different masks (Figs. 6(c), 6(d) and 6(e)). However, note that the method proposed by [13] only uses a mask obtained by a intensity threshold which corresponds to Fig.6(c).

Mean square error is shown in Fig. 7. Red dashed line is the best score that can be obtained computed between the ground truth (image without noise nor bias) and the image corrected by the known bias (thus only noise is present). Our method (black curve) obtains the best score for all window sizes, presenting a stable behavior for all of them. These results also show the importance of using a good mask in the correction process: the better the masking the lower the error. In our tests on real images (Fig. 3), the mask computed with our method covers the 75% of an ideal hand-segmented area, while miss-segmentation stays around 0.5% only.

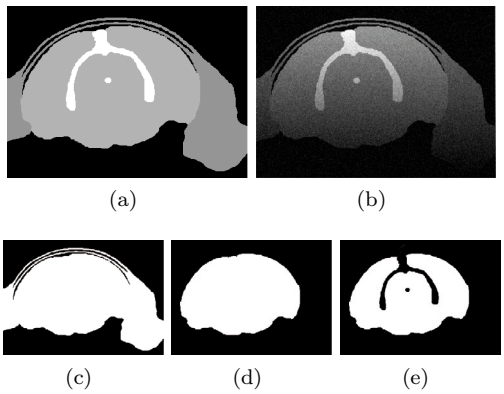

Figure 6: Ground truth simulated data (a), biased and noisy simulated data (b), Mask1 (c), Mask2 (d), Mask3 (e).

5.2 Real data

Our proposed methodology has been tested on 4 7-day old and 4 27-day old rat brains. Because of space limitation, results are shown for one data set only but similar results have been obtained for the rest of the images. Figure 8(a) shows the original 2D slice ($z = 12$), its intensity profile along vertical axis is plotted in Fig. 8(c),

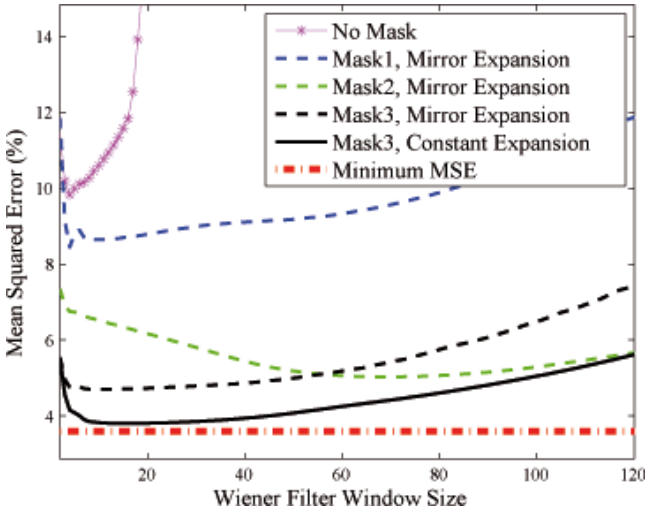

Figure 7: Mean Squared Error (in %) evaluation using the masks shown in Fig. 6, varying the window size of the Wiener Filter.

the corrected image and its intensity profile are shown in Figure 8(b) and (d) respectively. We use a Wiener filter of window size [20,20], which corresponds to the empirical optimal value obtained in Fig. 7. Visual inspection of the corrected image shows a more homogeneous intensity even if certain high frequency bias still remains (as seen in the upper part of the skull); as our basic assumption is the smooth behavior of the bias field, those zones remain biased after the correction. Intensity profile plots show however a good removal of low variation intensity, that is, the flattening of the profile. In fact, the method keeps the same noise level before and after the correction in the upper part of the image, and unavoidably enhances the noise in the lower part of the image where the SNR is much lower. In order to

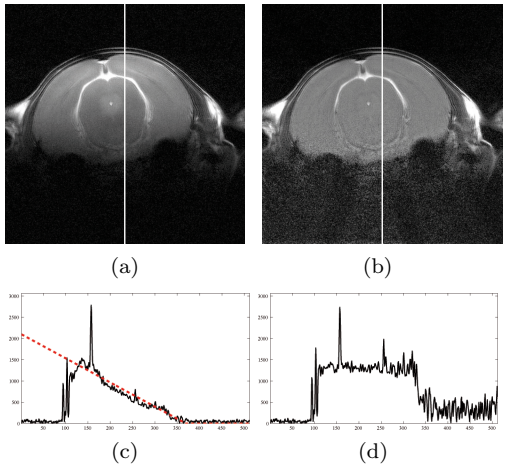

Figure 8: (a) original biased image, (b) bias corrected image, (c) Intensity profile of (a) and linear approximation of the bias(red slashed line), and (d) Intensity profile of (b).

check the robustness of the method in *3D*, the original

and bias corrected 3D volumes are shown in Figure 9. Here a Gaussian Filter of window size 50×50 pixels and $\sigma = 16$ pixels has been used. Intensity all over the rat brain is homogeneous in the axial, coronal and sagittal planes after the correction. We can even distinguish the right eye of the rat, which was hidden in the original image. Note however the little fading which appears in the extremes of z-direction, due to the lack of information on these sides, where the SNR was extremely poor (for instance in the zone where the left eye of the rat is).

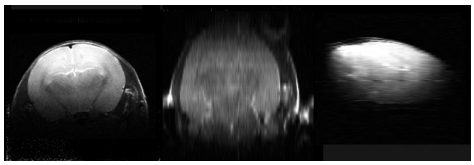

(a)

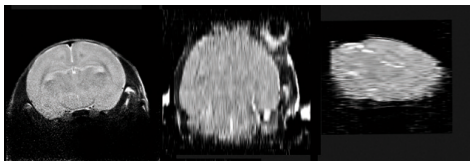

(b)

Figure 9: Three central projections of the original biased acquisition (a), and correction obtained (b).

6. DISCUSSION

We presented in this paper two pre-processing filters that overcome some of the current limitations of low-pass frequency models for bias correction in MR images. We focus our work to high-field ($9.4T$) surface coil brain images of the rat since the bias present on such data make their visual inspection and computer vision technique analysis very difficult if not impossible. The main advantage of the proposed method is that it can deal with higher bias variations, that is, more suited for high magnetic fields.

The proposed method has been designed to be as much automated as possible. Few parameters are needed (background and contour thresholds, structure element of the morphological operations) and, after testing on several images, they can be easily set. The proposed approach do not has high complexity and is fast. The computation time of the whole process (including both thresholds chosen by the user) is $2m40sec$[4]. This lapse of time corresponds to a Matlab implementation of the code, and can be certainly improved by means of a specific C++ implementation.

Only results using Wiener and Gaussian filters are shown in this paper. But any other low-pass frequency model could be used. Another advantage is that the presented approach requires little prior knowledge about the acquisition process since it does not rely on statistical information.

In this work we made the assumption of having an image single class object. Further work will focus on extending our solution to a multi-class case, as for instance a 7T MR image of the human brain containing gray matter and white matter. Finally, the validation present in this work remains qualitative. In a future work we are planning to quantitative assess our approach by imaging a *phantom* as well as by comparing surface coil correction with volume coil acquisitions (that present much less bias artifact). Finally, the advantages of other expansion techniques should be tested as well, such as inpainting methods[15], which uses diffusion of image intensities.

[4]Intel® Core™2 CPU, 6600@2.40GHz, 3.25 GB RAM.

REFERENCES

[1] P. Marzola et al., "High field MRI in preclinical research," Eur J Radiol, Vol. 48, No. 2, pp.165–70, 2003.

[2] E.M. Haacke et al., "Magnetic Resonance Imaging: Physical Principles and Sequence Design," Wiley Liss, 1999.

[3] Z. Hou, "A Review on MR Image Intensity Inhomogeneity Correction," International Journal of Biomedical Imaging, Vol. 2006.

[4] U. Vovk, "A Review of Methods for Correction of Intensity Inhomogeneity in MRI," IEEE Trans. on Medical Imaging, Vol. 26, No. 3, 2007.

[5] B.H. Brinkmann et al., "Optimized Homomorphic Unsharp Masking for MR Grayscale Inhomogeneity Correction", IEEE Trans. on Medical Imaging, Vol. 17, No. 2, 1998.

[6] F. Lin et al., "A wavelet-based approximation of surface coil sensitivity profiles for correction of image intensity inhomogeneity and parallel imaging reconstruction", Human Brain Mapping, vol. 19, no. 2, pp. 96-111, 2003.

[7] M. Styner et al., "Parametric Estimate of Intensity Inhomogeneities Applied to MRI", IEEE Trans. on Medical Imaging, vol. 19, no. 3, pp. 153 165, 2000.

[8] S. Geman and D. Geman, "Stochastic relaxation, Gibbs distributions, and the Bayesian restoration of images," IEEE Trans. on Pattern Analysis and Machine Intelligence, vol. 6, no. 6, pp. 721741, 1984.

[9] Y. Zhang et al, "Segmentation of brainMR images through a hidden Markov random field model and the expectation-maximization algorithm," IEEE Trans. on Medical Imaging, vol. 20, no. 1, pp. 4557, 2001.

[10] N. Dowell et al, "Fast, Accurate, and Precise Mapping of the RF Field In Vivo Using the 180 Signal Null", Magnetic Resonance in Medicine, Vol. 58, pp. 622-630, 2007.

[11] A. Fan, "A Variational Approach to MR Bias Correction" Master of Science in Electrical Engineering and Computer Science at the Massachusetts Institute of Technology, January 2003.

[12] M.S. Cohen, et al., "Rapid and Effective Correction of RF Inhomogeneity for High Field Magnetic Resonance Imaging", Human Brain Mapping, Vol. 10, No. 4, pp. 204–211, Jul 2000.

[13] H. Cheng et al., "MRI Image Intensity Correction with Extrapolation and Smoothing", Proceedings of the IEEE Engineering in Medicine and Biology 27th Annual Conference Shanghai, China, September 1-4, 2005.

[14] J. Haselgrove et al., "An algorithm for compensation of surface-coil images for sensitivity of the surface coil", Magnetic Resonance Imaging, Vol. 4, No. 6, pp. 469-472, 1986.

[15] M. Bertalmo et al., "Image Inpainting", Proceedings of SIGGRAPH 2000, New Orleans, USA, July 2000.